Video Article

Studying Triple Negative Breast Cancer Using Orthotopic Breast Cancer Model

Robert Y. S. Cheng[1], Nimit L. Patel[2], Timothy Back[1], Debashree Basudhar[1], Veena Somasundaram[1], Joseph D. Kalen[2], David A. Wink[1], Lisa A. Ridnour[1]

[1]Molecular Mechanism Section, Cancer and Inflammation Program, Center for Cancer Research, National Cancer Institute at Frederick

[2]Small Animal Imaging Program, Frederick National Laboratory for Cancer Research, Leidos Biomedical Research, Inc.

Correspondence to: Lisa A. Ridnour at ridnourl@mail.nih.gov

URL: https://www.jove.com/video/60316
DOI: doi:10.3791/60316

Keywords: Cancer Research, Issue 157, MDA-MB-231, orthotopic, metastasis, breast, cancer, TNBC

Date Published: 3/20/2020

Citation: Cheng, R.Y.S., Patel, N.L., Back, T., Basudhar, D., Somasundaram, V., Kalen, J.D., Wink, D.A., Ridnour, L.A. Studying Triple Negative Breast Cancer Using Orthotopic Breast Cancer Model. *J. Vis. Exp.* (157), e60316, doi:10.3791/60316 (2020).

Abstract

Triple-negative breast cancer (TNBC) is an aggressive breast cancer subtype with limited therapeutic options. When compared to patients with less aggressive breast tumors, the 5-year survival rate of TNBC patients is 77% due to their characteristic drug-resistant phenotype and metastatic burden. Toward this end, murine models have been established aimed at identifying novel therapeutic strategies limiting TNBC tumor growth and metastatic spread. This work describes a practical guide for the TNBC orthotopic model where MDA-MB-231 breast cancer cells suspended in a basement membrane matrix are implanted in the fourth mammary fat pad, which closely mimics the cancer cell behavior in humans. Measurement of tumors by caliper, lung metastasis assessment via in vivo and ex vivo imaging, and molecular detection are discussed. This model provides an excellent platform to study therapeutic efficacy and is especially suitable for the study of the interaction between the primary tumor and distal metastatic sites.

Video Link

The video component of this article can be found at https://www.jove.com/video/60316/

Introduction

Approximately one in eight women in the United States will develop invasive breast cancer during her lifetime, and 10%−20% of these women will be diagnosed with the aggressive triple negative breast cancer (TNBC) subtype. While primary lesions can be surgically removed in most cases, the subclinical micrometastasis and chemoresistance make it an intractable disease. Importantly, most patients with metastatic TNBC eventually relapse, even if they underwent treatment in the early stage[1]. Thus, cancer heterogeneity, micrometastasis, and therapeutic resistance are three major challenges limiting the successful clinical outcome of TNBC patients. Hence, there is an urgent need to better understand the polymorphic molecular background of TNBC and develop effective therapeutic agents that limit metastatic disease.

Tumor metastasis is a multistep process where the tumor cell controls and usurps its microenvironment to promote its own dissemination via membrane degradation and tumor cell escape from the primary lesion, via entry into (i.e., intravasation) and exit from (i.e., extravasation) the vasculature, and ultimately adaptation and colonization within distal tissue beds[2]. Animal models have been developed to study breast cancer metastasis, where two methodologies are commonly implemented: direct blood circulation injection and orthotopic implantation. Commonly employed methods for direct blood circulation injection include tail vein injection, while other approaches including direct cardiac injection[3], direct brain injection[4], and direct liver injection[5] have also been employed. The direct blood circulation injection is often referred to as an artificial metastasis model, which is quick and easy but less physiologically accurate because it circumvents tumor escape from the primary lesion and intravasation[6,7,8]. When compared to direct injection models, the orthotopic breast cancer model takes longer for the occurrence of detectable metastatic lesions in remote organs such as the lung, but it is more physiologically relevant because it closely mimics the multistep metastatic process as it occurs in humans. Importantly, a 2013 study[9] compared the tail vein injection and orthotopic models and found that the breast cancer cells injected into the tail vein and those isolated from lung metastatic lesions after tail vein injection exhibited similar global gene expression profiles. In contrast, the global gene expression profile of orthotopically injected breast cancer cells was dramatically different than that of lung metastatic lesions arising from orthotopically injected cells[9]. These observations suggest that the orthotopic model is more physiologically relevant, because the metastatic lesions undergo a selection process similar to the multistep process of metastasis as it occurs in humans.

This work describes an orthotopic breast cancer (MDA-MB-231-Luc/GFP) model in nude mice that was optimized in our laboratory for imaging detection techniques as well as the identification of novel biomarkers and development of targeted chemotherapeutic agents.

Protocol

Analysis of tumor growth was carried out using protocols approved by the Committee for the Ethics of Animal Experiments of the National Cancer Institute and adhered to the recommendations of the United States National Research Council's "Guide for the Care and Use of Laboratory Animals", the United States Public Health Service's "Guide for the Care and Use of Laboratory Animals", and the "Policy on Humane Care and Use of Laboratory Animals".

1. Preparation of cells for implantation

NOTE: MDA-MB-231 human breast adenocarcinoma cells (commercially acquired) were stably transfected with the luciferase gene III and enhanced green fluorescent protein (GFP) marker by lentivirus and grown in the presence of the selection antibiotic (puromycin).

1. Start the cell culture with 1 x 10^6 MDA-MB-231-Luc/GFP cells and add 15 mL of prewarmed (37 °C) RPMI 1640 medium with 10% fetal bovine serum (FBS) in a T75 culture flask. Keep the cells growing in a temperature-controlled cell culture incubator at 37 °C with 5% CO_2. Replace the complete medium at least 2x a week.
   NOTE: Do not disturb the cell growth and keep checking the cell growing conditions daily. The cells need to be subcultured when they reach 85%−90% confluency to maintain the proliferation phase.
2. One week before the cell implantation step, remove the puromycin from the cell culture flask by first removing all the medium in the culture flask, then rinsing 2x with 10 mL of 1x phosphate buffered saline (PBS), and finally replacing the medium with complete medium without the puromycin. During the medium-adding and rinsing steps, do not disturb the cells. Remember not to use the complete medium with the selection antibiotics from now on for all medium replenishment steps.
3. On the day of preparing the cells for implantation, remove all complete medium before trypsinization to avoid deactivating the trypsin. Add 5 mL of trypsin to the flask to trypsinize the cells. Monitor the cells and check that they detach from the culture flask.
4. Once the majority of the cells detach, add 10 mL of complete medium to neutralize the trypsin activity. Next, transfer the cell suspension to a 50 mL centrifuge tube and centrifuge at ~150 x *g* to pellet the cells. Remove the supernatant after the centrifugation and then add 10 mL of 1x PBS to resuspend the cells and prepare for cell counting.
5. Count the cells with a cell counter and adjust the cell concentration to 20 x 10^6 cells/mL in cold 1x PBS containing 25% basement membrane matrix. Inject 2 x 10^6 cells in 0.1 mL 1x PBS with 25% basement membrane matrix into the fourth mammary fat pad of each mouse. Bring extra needles and syringes for the cell implantation and keep the cell-basement-membrane-matrix mix on ice prior to implantation.
   NOTE: There is dead space in the syringe and needle. Depending on the choice of needle and syringe length, type, and size, a tuberculin syringe with a 0.5 in 26 G needle can have up to 70 µL dead space[10]. Prepare 40%−50% more cell implantation mix to compensate for the dead space and any other accidental loss.

2. Orthotopic breast cancer model and tumor size measurement

1. Allow 6-week-old female athymic nude mice to acclimate to the housing facility for at least 1 week before the cell implantation.
   NOTE: Using same age mice will reduce data variation.
2. For each round, anesthetize five mice with isoflurane at 4% with filtered (0.2 µm) air at a flow rate of 1 L/min for 3−4 min. Pay attention to the mouse respiratory rate and pattern change, and use a toe pinch to ensure that the mice are under proper anesthesia. Once they are no longer moving, remove one mouse and place a nose cone over its nose and mouth with the same anesthesia.
3. Swab the left 4th mammary gland with alcohol. Using fine rat tooth forceps, lift the 4th mammary gland slightly to insert the 25 G needle. Make sure the needle is bevel up and then slightly pull the plunger to make sure the needle does not hit any blood vessels. If no blood enters the syringe, continue to slowly inject 100 µL of the cell-basement-membrane-matrix mix into the mammary fat pad.
   NOTE: A round, raised area will appear underneath the skin.
4. Wait 10−15 s for the basement membrane matrix to harden, then remove the needle. Repeat the process with the remaining mice in the induction chamber. Place all used needles and syringes in a sharp box.
5. Use the same mammary gland injection site for all mice. Keep a close eye on the injection site and note any cell implantation mix leaking out from the injection site.
   NOTE: Within a few minutes, the mouse will start to regain consciousness.
6. Allow the xenograft to grow freely without any interruption for 7−10 days prior to any tumor size measurement.
7. Examine all mice for the xenograft size. Measure the tumor size with a caliper. Determine the tumor volume (mm^3) with the following equation:
   $$\frac{L \times W \times W}{2} = Tumor\ Volume$$
   where L is the longest dimension and W is the shortest dimension perpendicular to L.
8. Identify and remove outliers exceeding one standard deviation of the mean. Only use mice with comparable tumor sizes for experiments. Randomly divide the mice into different treatment groups and begin treatments.
9. Measure the tumor size by caliper 2x a week. Keep note of all the physical changes of the xenografts (i.e., necrosis, laceration).

3. In vivo bioluminescence and ex vivo fluorescence imaging

NOTE: In this study, both two-dimensional bioluminescence and fluorescence imaging are conducted at the endpoint of the experiment. The bioluminescence imaging (BLI) was performed using a commercial preclinical optical scanner equipped with a 16-bit cooled CCD camera and heated imaging stage.

1. Before imaging, anesthetize up to five tumor-bearing mice in the induction chamber by setting isoflurane at 3% with filtered (0.2 µm) air at a flow rate of 1 L/min for 3−4 min. Determine anesthesia by a toe pinch. Ensure that the induction chamber is kept inside a vented hood to minimize staff exposure to isoflurane.
2. Administer D-luciferin (150 mg/kg) to the anesthetized mice by an intraperitoneal route using a 27 G needle, and transfer an anesthetized mouse to the imaging chamber. At the scanner imaging chamber, maintain the isoflurane at 2%−2.5% with O_2 as a carrier with a flow rate of 1 L/min.
   NOTE: Maintain the body temperature of the mouse at ~37 °C during the procedure by keeping a heated pad under the anesthesia induction chamber, imaging table (if the stage is not heated), and postprocedure recovery cage.
3. Before imaging the study mice, obtain luciferin kinetics by imaging three extra tumor bearing mice (animals not assigned to any study groups) at 2 min intervals for a total of 40 min using the following parameters: excitation filter-blocked, emission filter-open, f/stop 1, FOV-D, medium binning (8 x 8), and auto exposure. Use the peak bioluminescence signal measured to define the optimal image acquisition time window for all subsequent time points.
4. While performing metastasis imaging, shield the high BLI signal from the primary tumor by covering it with a sleeve cut out from a black glove. Acquire the image using the same parameters described in step 3.3 with the ventral side of the mouse facing the camera for lung metastasis imaging and the dorsal side of the mouse facing the camera for the brain metastasis imaging.
   NOTE: It is essential to test a few different brands of black gloves to pick the one with minimal auto luminescence.
5. Using a scanner and data analysis software, draw a standard shape region of interest (ROI) over the thoracic cavity or the brain ensuring that the entire organ of interest is covered to evaluate the metastatic burden. Quantify the bioluminescence (BL) output as total flux (photons/second).
6. Immediately after BLI, euthanize the mouse via CO_2 asphyxiation (as per ACUC guidelines and institution-approved animal protocols) and extract the lung and the brain with dissecting scissors and forceps for ex vivo imaging.
   NOTE: The lung extracted for ex vivo imaging and for lung metastasis nodule counting cannot be performed on the same mouse due to incompatible procedures.
7. Quickly rinse all organs with 1x PBS to remove any superficial bloodstains and place organs on a low-autofluorescence, black plastic plate. Transport organs to a multispectral fluorescence scanner equipped with spectral unmixing capability (solid-state liquid crystal wavelength tuning) with a 12-bit CCD camera for GFP detection.
8. Acquire multispectral GFP images (excitation filter = 457 ± 23 nm; emission filter = 490 nm long pass) of the extracted organs and non-tumor bearing control mice by scanning through 500−720 nm at a step size of 10 nm. Use excised organs from non-tumor bearing control mice to correct for autofluorescence.
9. After multispectral GFP imaging, determine the optimal imaging settings. Perform image acquisition of all target organs and conduct image analysis (i.e., generate a spectral library for autofluorescence and GFP for spectral unmixing procedure) according to the manufacturer's protocol.

4. Molecular detection of metastatic breast cancer cells

1. After the ex vivo imaging, snap freeze the whole brain in liquid nitrogen and store at -80 °C in a freezer until ready for the DNA extraction.
2. For DNA extraction, put the whole brain in a 5 mL homogenizing tube with 2 mL of DNA lysis buffer. Use a homogenizer with the power setting at 50 to homogenize the snap-frozen whole brain tissue. Once the brain tissue is totally homogenized, transfer the 1 mL suspension (lysate) to a DNase-free and RNase-free 2 mL microcentrifuge tube and continue to isolate the DNA according to the manufacturer's protocol.
   NOTE: To minimize carryover DNA contamination, thoroughly clean the homogenizer after each sample by first rinsing it with 75% ethanol in DNase-free and RNase-free water, then rinsing with 1 M NaOH solution, followed by a rinse with 75% ethanol in DNase-free and RNase-free water to effectively reduce and destroy any DNA residue.
3. Add 0.5 mL of 100% ethanol of DNA lysis buffer to the lysate. Mix sample by inversion and store at room temperature for 3 min.
   NOTE: Do not invert too many times or too vigorously. The DNA will be visible as a wool-like precipitate.
4. Use a pipette tip to transfer the DNA to a fresh DNase-free and RNase-free 2 mL microcentrifuge tube. Let the sample air dry for 1 min. Add 1 mL 75% ethanol and invert the microcentrifuge tube 3−6x to wash the DNA sample. Discard the ethanol after each wash by pipetting. Repeat the wash step 2x.
5. Air dry the DNA sample for 10 s. Then add 52 µL of 8 mM NaOH to dissolve the DNA sample. Pipet 2 µL of the DNA sample for DNA quantitation, and use the remaining 50 µL for a real-time PCR assay after concentration adjustment.
   NOTE: NaOH helps to fully solubilize the DNA sample.
6. Quantitate 2 µL of each DNA sample with a spectrophotometer and use an absorbance ratio between A260/280 as a quality check reference. Calculate the DNA concentration with this formula:
   $$\text{dsDNA concentration} = 50\ \mu g/mL \times OD_{260} \times \text{dilution factor}$$
7. Adjust the DNA concentration to 50 ng/µL. For each DNA sample, use 50 ng of DNA as the starting template for a real-time PCR assay. Use 8 mM NaOH solution or DNase-free and RNase-free water to dilute the DNA sample.
8. Design the primer pair specific to the exogenous green fluorescence protein (GFP) sequence in-house using an open source primer design web portal for real-time PCR detection of the GFP tag in the metastatic cells that invaded and colonized distal sites.
   NOTE: This study used F: 5'-AGAACGGCATCAAGGTGAAC-3', R: 5'-TGCTCAGGTAGTGGTTGTCG-3'.
9. Use a fast real-time PCR reagent and a real-time PCR machine that supports a fast real-time PCR protocol. In addition to the regular 30 cycle amplification steps, add a dissociation curve step to the end of the run for the detection of any nonspecific amplification.
   NOTE: The following conditions were used for molecular detection: 95 °C 2 min hot start, 40 cycles of 95 °C 5 s, 60 °C 15 s, and lastly a melting curve analysis. The GFP amplicon is 135 bp in size.
10. Use a naive mouse brain DNA (not a MDA-MB-231 cell implant) as a negative control. Use DNA extracted from the MDA-MB-231-GFP/Luc cells as a positive control. Add all the PCR reagents without any DNA template as a no template control (NTC).
    NOTE: A PCR control is needed for each PCR assay.

5. Metastatic breast cancer cell detection in lung

1. For the mice subgroup chosen for the metastatic lung nodule counting, anesthetize mice with isoflurane (as in step 2.2) immediately after the ex vivo imaging, perform a cardiac puncture for blood collection, and then euthanize by cervical dislocation.
2. Open the chest cavity with dissecting scissors and cut past the heart and thymus to expose the trachea.
3. Insert a 10 mL syringe with a 22 G needle containing Bouin's solution into the trachea. Push the syringe plunger until the collapsed lungs are swollen with ~2 mL of the Bouin's solution. Remove the syringe and needle once the lungs have been inflated.
4. Place the whole lung into a 15 mL tube containing Bouin's solution, gently invert the tube a few times, and allow to soak for 24 h at room temperature.
5. After 24 h, remove the Bouin's solution from the tube, rinse the lung with water, and then place it back in the tube with 70% ethanol. Count metastasis (white patches or nodules) on the surfaces of the lungs using a dissecting microscope.

6. Data collection and analysis

1. Record tumor volume data, as well as in vivo and ex vivo imaging data, on an electronic spreadsheet for easy data entry, collection, and management.
2. At the end of the experiment, transfer all data to the electronic spreadsheet and statistical software for data plotting and statistical analyses.

Representative Results

Tumor volume measurement by caliper is a well-established method to assess treatment efficacy (**Figure 1**). The number of cells implanted, use of basement membrane matrix, microbiome, facility cleanliness, and injection site are the key factors impacting the tumor growth rate.

Unlike the GFP imaging, BLI required the administration of luciferase substrate at least 15−20 min prior to BLI imaging. Furthermore, the mouse strain, cell line, treatments, and luciferase reporter all affect the bioluminescence signal levels. Thus, to obtain comparable signals between the study groups, a pre-imaging BLI kinetic study must be conducted to determine the best imaging time frame (**Figure 2**).

Due to the superior signal-to-background ratio[26,27], the whole body in vivo bioluminescence imaging was quite sensitive in detecting low-level metastasis signal compared to the GFP approach (**Figure 3**). Furthermore, the bioluminescence signal provided deeper penetration than GFP by a few millimeters. However, bioluminescence signal production requires ATP, which is a limiting factor in evaluating ex vivo tissue samples. If the animals are processed quickly, then BLI could be a viable approach to obtain quantitative results on metastasis. One way to achieve this is by processing one animal at a time. However, this approach was not feasible for this study because a large cohort of mice was used. BLI signal was not detected when the organs were imaged around 45 min post luciferin injection. The use of a dual reporter cell line is useful in this situation. Due to the stable nature of the GFP molecule, researchers would have sufficient time to process the carcass prior to capturing the GFP signals from target organs (**Figure 4**).

Figure 5 provides a real-life example of how caliper tumor size measurements could distort the data interpretation, because the xenograft lost most of the viable tumor cell content but still maintained its large mass and shape. Histopathological examination of those xenografts indicated necrosis inside the mass (**Figure 5B**).

For researchers who challenge the imaging results regarding the brain metastasis in the orthotopic breast cancer model, molecular detection by real-time PCR can provide convincing evidence (**Figure 6**). In this case, the exogenous GFP DNA sequence was the best way to address this problem, because the transfected GFP DNA sequence does not naturally exist in humans or rodents.

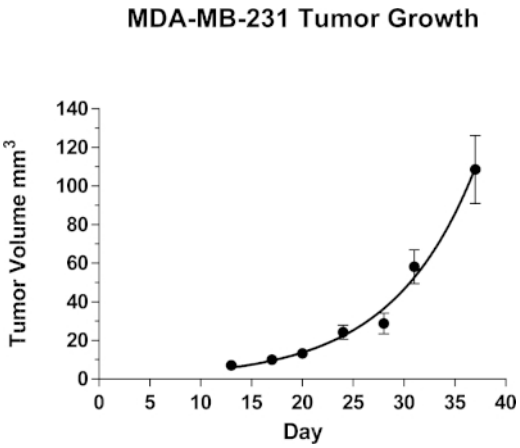

Figure 1: Tumor volume measurement. Tumor volume/loading measurement with a caliper started on day 10 after xenograft implantation and then was measured 2x a week until the end of the experiment. Error bars are calculated by SEM value. Please click here to view a larger version of this figure.

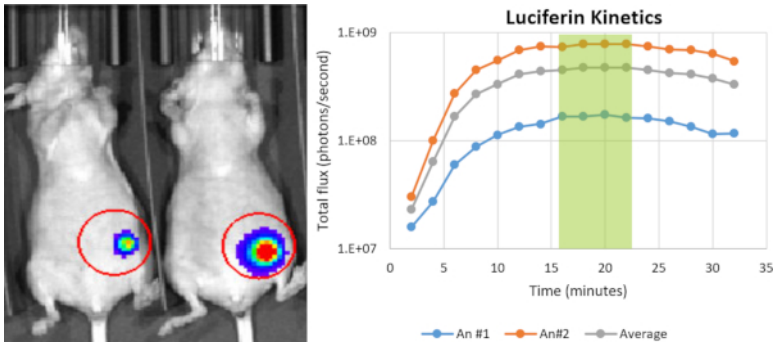

Figure 2: Determination of optimal image acquisition window. Left: One mouse with a large xenograft and one mouse with a small xenograft were selected for the optimal luciferin kinetic range determination. Right: Luciferin kinetic curve obtained by acquiring the images every 2 min for 40 min. A plateau was observed between 15−22 min, which was used as an optimal image acquisition time for all subsequent imaging. Please click here to view a larger version of this figure.

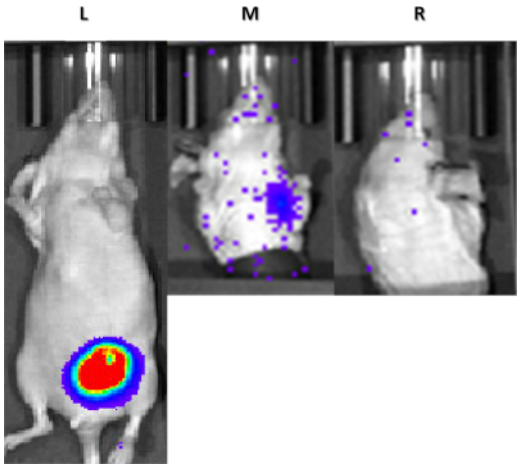

Figure 3: Whole body BLI imaging. L: Whole body BLI imaging. M: Ventral view with the lower body covered with a sleeve of a black glove. R: Dorsal view with the lower body covered with a sleeve of a black glove. An axillary lymph node metastasis is detected in the ventral view by BLI imaging. Please click here to view a larger version of this figure.

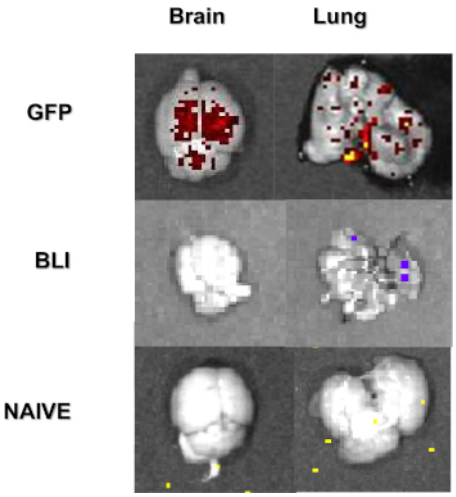

Figure 4: Ex vivo BLI/GFP signal detection. GFP signals were detected in the brain and lung from the same mouse 20 min after the mouse was sacrificed. BLI signal was not detected 45 min post luciferin injection. No GFP signal was detected in naive mouse brain and lung. Please click here to view a larger version of this figure.

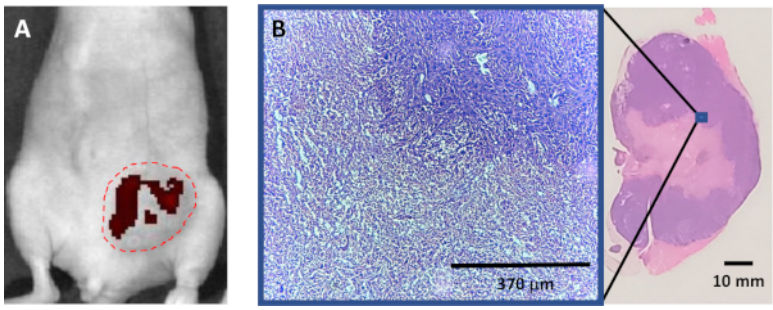

Figure 5: Advantages of optical imaging techniques over caliper measurements. (**A**) Representative image showing in vivo GFP signal detection in a primary tumor. Only a minor portion of the xenograft showed GFP signal, suggesting that a significant portion of the mass was stroma. This cannot be determined by traditional caliper measurements and can lead to an inaccurate conclusion. This example highlights the importance of optical imaging for the animal model study. (**B**) Histopathology section of the same mouse showing that the necrotic region (i.e., inner region) also contributed to the tumor size calculation. Please click here to view a larger version of this figure.

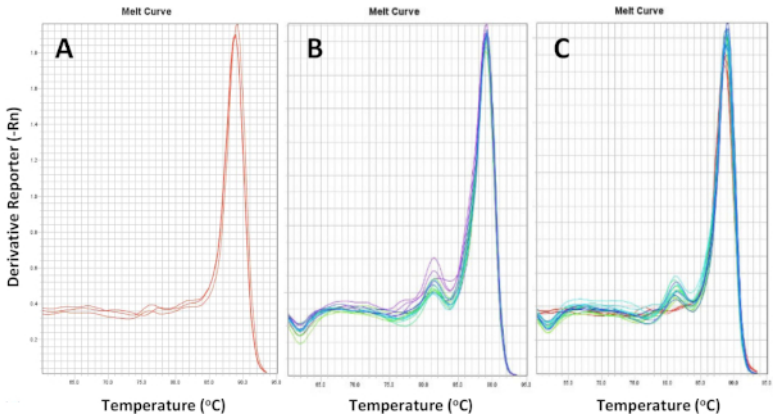

Figure 6: Melting curve analysis. The melt curve plot showing the specificity of GFP amplicons. DNA from the brain obtained from the MDA-MB-231-Luc/GFP-implanted mice and the DNA isolated from the MDA-MB-231-Luc/GFP cells grown in culture (positive control) were assayed. The real-time PCR assay was performed to assess the GFP content in the brain tissue. (**A,B**) The melting curves of the positive control and the DNA extracted from mouse brain, respectively. (**C**) The overlapped curves of panels A and B, indicating the peak signals from the mouse brain DNAs are specific for the exogenous GFP sequence. Please click here to view a larger version of this figure.

Discussion

For the study of TNBC in animals, two murine models have been developed: the MDA-MB-231 human breast adenocarcinoma cells in immune-compromised mice (i.e. athymic nude mice, NSG mice), and the 4T1 in immune-competent BALB/c mice. Both models have their advantages. The choice of the animal model for a study depends on the research goals. For example, the MDA-MB-231 model is a human TNBC cell line grown in immunocompromised mice that mimics immunosuppressed human breast cancer patients. On the other hand, the invasive phenotype of orthotopic 4T1 triple-negative murine breast cancer cells in BALB/c mice closely mimics the metastatic process as it occurs in stage IV human breast cancer patients. Unlike the intravenous cell injection approach, human MDA-MB-231 breast cancer cells were similarly injected into the mammary fat pad[11,12] in the orthotopic breast cancer model[11,13]. The longer tumor growth and the acquired metastatic ability is more physiologically relevant, thus it is not an artificial metastatic cancer model[4,14]. Such a spontaneous metastasis model closely mimics human breast cancer development except for the initiation stage. This is a crucial model for in vivo drug screening and therapeutic efficacy assessment in metastatic breast cancer.

The tumor implantation site in the mouse plays a crucial role in providing a microenvironment that sustains tumor growth and the selection of metastatic phenotype similar to that which occurs in humans. The proximal lymph node and the presence of adipose tissue are the key factors affecting the disease progression of breast cancer[15,16]. In a human patient, the lymph node and adipose tissue are both key interacting factors affecting the malignancy and incidence of breast cancer[17,18,19]. Thus, the selection of the correct anatomical location for the injection site can highly impact the relevancy of the tumor model compared to the human disease. This study used the fourth mammary gland as the implantation site mainly due to the aforementioned requirements and that it is anatomically more accessible and easier to manipulate.

Different tumor volume calculation methods are available, and a researcher can choose any they see fit. The algorithm selected for this study is based on the findings by Faustino-Rocha et al., who compared different tumor volume calculation formulas and concluded that the formula below is the most accurate[20].

$$\frac{L \times W \times W}{2} = Tumor\ Volume$$

Basement membrane matrix is an important extracellular matrix used in various in vitro[21] and in vivo[22,23] assays. There are contradicting reports[22,24,25] regarding the influence of the basement membrane matrix on xenograft malignancy. It seems to only affect the initial establishment of the xenograft and have no further effect on xenograft growth[25]. For the xenograft implantation described, the basement membrane matrix was

mixed with the cancer cells to increase the cell/gel mix solution viscosity prior to implantation. The presence of the basement membrane matrix reduces the loss of mix solution from the injection site and keeps the mix solution at the implantation site, thus increasing the uniformity of the implanted xenograft volume.

The MDA-MB-231 cell line is a malignant immortalized human breast adenocarcinoma cell line and is a popular tool in breast cancer research because of its triple-negative status. The use of dual reporters (luciferase and GFP) cell line allows more flexibility in handling the in vivo and ex vivo imaging. It is well established that the bioluminescence signal possesses greater sensitivity, depth detectability, and superior contrast (signal-to-noise ratio) than GFP signals. Because of this, it is a widely used imaging modality for whole body imaging. Unfortunately, bioluminescence detection is limited by a narrow time window (~15−20 mins post luciferin injection) during which the signal detection is linear. BLI signal diminishes rapidly when the animals are euthanized. This becomes an experimental design issue if many mice need to be euthanized and harvesting multiple tissues or organs is required. In these studies, blood was harvested by direct heart puncture, the brain, primary tumor, lung, and affected lymph node were examined in 40 mice. By the time the organs were harvested and ready for ex vivo imaging, the bioluminescence signal was undetectable. Therefore, GFP detection is more suitable in these situations. The emission of the GFP signal is in the visible range, and at these wavelengths, signal absorption due to blood (i.e., hemoglobin) is significantly higher. Also, autofluorescence in the visible range due to NADH, lipo-pigments, and flavins results in a significant background that makes it difficult to distinguish between a low-level GFP signal and autofluorescence background. Employing a multispectral fluorescence imaging approach instead of traditional filter-pair imaging and using spectral unmixing algorithms helps identify true GFP signal in the organ of interest. Hence, by combining the strengths of bioluminescence imaging in whole body in vivo detection and multispectral GFP imaging in the ex vivo organ/tissue evaluations, quantifiable data can be maximized in a large cohort of mice.

No matter which approach is selected for an animal study, extracting all blood prior to organ/tissue retrieval is highly recommended, especially for studies targeting the metastatic burden. This protocol detects GFP signals from the whole blood samples obtained from the mice (data not shown) in the orthotopic breast cancer model by real-time PCR assays. Minimizing the blood volume in organs/tissues will reduce the false positive signal in the target organs.

In conclusion, the orthotopic breast cancer model using the MDA-MB-231-Luc/GFP cells is a highly relevant animal model that closely mimics the human TNBC patient condition. This model is essential for studying, monitoring, and assessing therapeutic efficacy in a tumor microenvironment similar to human beings. The use of dual reporter cell lines further enhances the practicality of this orthotopic breast cancer model.

Disclosures

The authors have nothing to disclose.

Acknowledgments

The authors would like to acknowledge support by the Intramural Research Program of the National Institutes of Health, National Cancer Institute, Bethesda MD, Cancer and Inflammation Program, and the Frederick National Laboratory - Small Animal Imaging Program, Leidos Biomedical Research, Inc, Frederick Maryland, USA.

References

1. Abramson, V. G., Lehmann, B. D., Ballinger, T. J., Pietenpol, J. A. Subtyping of triple-negative breast cancer: implications for therapy. *Cancer.* **121**, 8-16 (2015).
2. Zhuang, X., Zhang, H., Hu, G. Cancer and Microenvironment Plasticity: Double-Edged Swords in Metastasis. *Trends in Pharmacological Sciences.* **40** (6), 419-429 (2019).
3. Campbell, J. P., Merkel, A. R., Masood-Campbell, S. K., Elefteriou, F., Sterling, J. A. Models of bone metastasis. *Journal of Visualized Experiments.* (67), e4260 (2012).
4. Saha, D., et al. In vivo bioluminescence imaging of tumor hypoxia dynamics of breast cancer brain metastasis in a mouse model. *Journal of Visualized Experiments.* (56), e3175 (2011).
5. Goddard, E. T., Fischer, J., Schedin, P. A Portal Vein Injection Model to Study Liver Metastasis of Breast Cancer. *Journal of Visualized Experiments.* (118), e54903 (2016).
6. Lim, E. et al. Monitoring tumor metastases and osteolytic lesions with bioluminescence and micro CT imaging. *Journal of Visualized Experiments.* (50), e2775 (2011).
7. Bauerle, T., Komljenovic, D., Berger, M. R., Semmler, W. Multi-modal imaging of angiogenesis in a nude rat model of breast cancer bone metastasis using magnetic resonance imaging, volumetric computed tomography and ultrasound. *Journal of Visualized Experiments.* (66), e4178 (2012).
8. Katsuta, E., Oshi, M., Rashid, O. M., Takabe, K. Generating a Murine Orthotopic Metastatic Breast Cancer Model and Performing Murine Radical Mastectomy. *Journal of Visualized Experiments.* (141), e57849 (2018).
9. Rashid, O. M. et al. Is tail vein injection a relevant breast cancer lung metastasis model? *Journal of Thoracic Disease.* **5**, 385-392 (2013).
10. Bhambhani, V., Beri, R.S., Puliyel, J.M. Inadvertent overdosing of neonates as a result of the dead space of the syringe hub and needle. *Archives of Disease in Childhood: Fetal and Neonatal Edition.* **90**, F444-445 (2005).
11. Zhang, G. L., Zhang, Y., Cao, K. X., Wang, X. M. Orthotopic Injection of Breast Cancer Cells into the Mice Mammary Fat Pad. *Journal of Visualized Experiments.* (143), e58604 (2019).
12. Tavera-Mendoza, L. E., Brown, M. A less invasive method for orthotopic injection of breast cancer cells into the mouse mammary gland. *Laboratory Animals.* **51**, 85-88 (2017).

13. Paschall, A. V., Liu, K. An Orthotopic Mouse Model of Spontaneous Breast Cancer Metastasis. *Journal of Visualized Experiments.* (114), e54040 (2016).
14. Kocaturk, B., Versteeg, H. H. Orthotopic injection of breast cancer cells into the mammary fat pad of mice to study tumor growth. *Journal of Visualized Experiments.* (96), e51967 (2015).
15. Fletcher, S. J., et al. Human breast adipose tissue: characterization of factors that change during tumor progression in human breast cancer. *Journal of Experimental and Clinical Cancer Research.* **36**, 26 (2017).
16. Giuliano, A. E., et al. Axillary dissection vs no axillary dissection in women with invasive breast cancer and sentinel node metastasis: a randomized clinical trial. *Journal of the American Medical Association.* **305**, 569-575 (2011).
17. Rummel, S., Hueman, M. T., Costantino, N., Shriver, C. D., Ellsworth, R. E. Tumour location within the breast: Does tumour site have prognostic ability? *Ecancermedicalscience.* **9**, 552 (2015).
18. Kroman, N., Wohlfahrt, J., Mouridsen, H. T., Melbye, M. Influence of tumor location on breast cancer prognosis. *International Journal of Cancer.* **105**, 542-545 (2003).
19. Bao, J., Yu, K. D., Jiang, Y. Z., Shao, Z. M., Di, G. H. The effect of laterality and primary tumor site on cancer-specific mortality in breast cancer: a SEER population-based study. *PLoS One.* **9**, e94815 (2014).
20. Faustino-Rocha, A. et al. Estimation of rat mammary tumor volume using caliper and ultrasonography measurements. *Lab Animal.* **42**, 217-224 (2013).
21. Mullen, P. The use of Matrigel to facilitate the establishment of human cancer cell lines as xenografts. *Methods in Molecular Medicine.* **88**, 287-292 (2004).
22. Jensen, R. L., Leppla, D., Rokosz, N., Wurster, R. D. Matrigel augments xenograft transplantation of meningioma cells into athymic mice. *Neurosurgery.* **42**, 130-135; discussion 135-136 (1998).
23. Mullen, P., Langdon, S. P. The use of matrigel in the establishment of ovarian carcinoma cell lines as xenografts. *Methods in Molecular Medicine.* **39**, 199-203 (2001).
24. Fliedner, F. P., Hansen, A. E., Jorgensen, J. T., Kjaer, A. The use of matrigel has no influence on tumor development or PET imaging in FaDu human head and neck cancer xenografts. *BMC Medical Imaging.* **16**, 5 (2016).
25. Mullen, P., Ritchie, A., Langdon, S. P., Miller, W. R. Effect of Matrigel on the tumorigenicity of human breast and ovarian carcinoma cell lines. *International Journal of Cancer.* **67**, 816-820 (1996).
26. Zinn, K. R., et al. Noninvasive bioluminescence imaging in small animals. *Journal of the Institute for Laboratory Animal Research.* **49**, 103-115 (2008).
27. Troy, T., Jekic-Mullen, D., Sambucetti, L., Rice, B. Quantitative Comparison of the Sensitivity of Detection of Fluorescent and Bioluminescent Reproters in Animal Models. *Molecular Imaging.* **3** (1), 9-23 (2004).